Effect of potential screening on the H_2 autoionizing states

Andrés Felipe Ordóñez-Lasso,[1,*] José Luis Sanz-Vicario,[2,†] and Fernando Martín[1,3,4]
[1]*Departamento de Química, Módulo-13, Universidad Autónoma de Madrid, 28049 Madrid, Spain*
[2]*Grupo de Física Atómica y Molecular, Instituto de Física, Universidad de Antioquia, 050010 Medellín, Colombia*
[3]*Condensed Matter Physics Center (IFIMAC), Universidad Autónoma de Madrid, 28049 Madrid, Spain*
[4]*Instituto Madrileño de Estudios Avanzados en Nanociencia (IMDEA-Nano), Cantoblanco, 28049 Madrid, Spain*
(Received 15 August 2017; published 9 November 2017)

We study the behavior of autoionizing states of the hydrogen molecule subject to screened Coulomb interactions using an *ab initio* Feshbach configuration interaction method. Special attention is given to the algorithms developed for the evaluation of (i) screened molecular orbitals expressed in terms of one-center expansions using B-spline polynomial basis functions and (ii) screened two-electron integrals between configurations expressed in terms of such molecular orbitals, by solving the screened Poisson equation. As an illustration of the method we focus on the lowest Feshbach resonance of the $\mathcal{Q}_1\ ^1\Sigma_g^+$ series of doubly excited states of H_2, which lies between the first H_2^+ $(1s\sigma_g)$ and the second H_2^+ $(2p\sigma_u)$ ionization thresholds. We show that Coulomb screening in the electron-proton interaction and between electrons may significantly alter the resonance position and autoionizing decay as a function of internuclear distance. In general, screening increases the resonance lifetime. However, when electron-proton screening dominates over electron-electron screening, we find that the $\mathcal{Q}_1$ resonance acquires a pronounced shape-resonance character at internuclear distances where the resonance approaches the lower ionization threshold, thus leading to a pronounced decrease of its lifetime.

DOI: 10.1103/PhysRevA.96.052503

I. INTRODUCTION

The screening of Coulomb interactions appears as a fundamental concept that arises ubiquitously in the electronic structure of many-body systems, from atoms to molecules, from clusters to metals, and from plasma to electrochemical environments. The screening of the long-range Coulomb forces in those systems may produce effects on their structure and dynamics, still unexplored or unexpected. For instance, the electroweak addition to the interaction between electrons and nuclei mediated by the exchange of a boson (still to be measured in high-precision atomic spectroscopy) has the form of a Yukawa potential. In this work we are interested in screening effects on few-body molecular systems. For instance, there is already a vast literature on plasma screening in atoms, and specifically in the analysis of superexcited resonance states in two-electron atoms (see [1] and references therein). On the contrary, screening effects on molecular resonance states have not been addressed so far, even in the most simple case of two-electron diatomic molecules.

The coupling constant for a plasma (ratio between the average Coulomb-interaction energy and the average kinetic energy) that obeys the classical statistics at temperature T is $\gamma = (Ze)^2/k_BTa$, where Z is the atomic charge, k_B is the Boltzmann constant, and $a = (4n/3)^{-1/3}$ is Wigner-Seitz radius of the ion sphere with volume $1/n$ [2]. Classical plasmas with $\gamma \ll 1$ are named weakly coupled plasmas. Screening in this case may be appropriately accounted for with the Debye-Hückel model [3]. In this model, the screening parameter can be expressed in terms of the density and the temperature of the plasma in the form $\lambda = [4\pi(Ze)^2 n/k_BT]^{1/2}$. Since this screening parameter depends on the ratio between the plasma density n and temperature, the same λ value can meet the conditions of a variety of plasmas. In the present study of resonances in H_2, the values for λ are limited within the range [0,0.25], since beyond the upper limit the Feshbach resonant states lying below the second ionization threshold cease to exist.

Our results may be useful in the analysis of weakly ionized molecular plasmas, under conditions of weak coupling with medium-high temperatures and high densities (hot dense plasmas), and for those cases in which the Debye approximation for a plasma remains valid [2,4]. These conditions may be met in laser-produced plasmas, stellar atmospheres, or at the edges of Tokamaks in the inertial confinement fusion, where the molecular hydrogen H_2 and its ionized form H_2^+ are typical chemical species. In these plasmas electron-molecule collisions take place as a fundamental process. In this respect, resonances in H_2 can be readily formed by collisions of low-energy electrons with the parent molecular ion H_2^+.

Very recently, we have explored the simplest of all molecules, H_2^+, subject to screened Coulomb interactions and we have found unreported shape resonances, Borromean states, and an unusual Stark mixing at intermediate internuclear distances [5]. In the simple Debye-Hückel approximation, screening is described by replacing the Coulomb potentials by Yukawa-like potentials ($V = q_iq_je^{-\lambda r_{ij}}/r_{ij}$) for each pair of charged particles $\{q_i,q_j\}$ separated by a distance r_{ij}. The lack of exactly solvable problems, including screening effects, has been perhaps the reason for the little attention paid in the literature to solve, from first principles, complex molecular systems under the effect of screening interactions. Moreover, the vast majority of molecular computational packages are based on (one-center and multicenter) molecular integrals with Coulomb interactions. Only a few works have dealt with these integrals in molecules. Previous work has

*Present address: Max Born Institute, 12489 Berlin, Germany.
†Corresponding author: jose.sanz@udea.edu.co

made use of (multicenter) Gaussian basis functions to evaluate screened nuclear attraction and electron repulsion molecular integrals [6]. This methodology has been used to study the variation of the ground-state energy of the hydrogen molecule under Yukawa screening by using full configuration interaction methods (FCI) [7].

In this work we are interested in superexcited states that lie in the electronic continuum, for which Gaussian basis sets are not well suited in general, since they are not able to describe their asymptotic oscillatory behavior. Instead we use one-center B-spline basis functions (piecewise polynomials) enclosed in a large electronic box. Thus, a big deal of attention is invested here in devising an efficient and accurate method for the evaluation of screened nuclear attraction and two-electron integrals using one-center molecular orbitals described with B-splines. With this aim, we have extended a method previously designed for pure Coulomb interactions [8,9] by solving the corresponding Poisson equation for an auxiliary function entering in the two-electron integrals. In this work we derive the radial screened Poisson equation and its corresponding solution for the screened case. This procedure has been introduced in our suite of molecular configuration interaction codes [10], reducing the computational effort by orders of magnitude against a direct numerical evaluation of the screened integrals.

To give support to our method of solution, we have applied it to the analysis of the lowest lying, doubly excited state of the $\mathcal{Q}_1\ ^1\Sigma_g^+$ Rydberg series, for which resonance parameters, energies, and widths are computed under different conditions for the electron-proton and electron-electron screenings. The variation of the resonance parameters with the amount of screening is understood by means of simple models, which also provide effective potentials that, under specific screening conditions, can exhibit potential barriers for the continuum electron.

The paper is organized as follows. In Sec. II we describe our methodology. The first part is devoted to the construction of screened molecular orbitals (Sec. II A), the second one to the method for calculating energies and widths for molecular resonance states (Sec. II B), and the third one to the method developed to compute screened two-electron repulsion integrals (Sec. II C). In Sec. III we apply these methods to study the lowest molecular resonance in H_2 under different screening conditions. We end up with some conclusions in Sec. IV. Atomic units (a.u.) are used throughout unless otherwise explicitly stated.

II. THEORY

We are interested in how screening effects affect the physics of molecular resonance states. These states, although partially localized in space, belong to the molecular electronic continuum. Here we solve the nonrelativistic electronic Schrödinger equation for a two-electron diatomic system AB (we firstly assume the validity of the Born-Oppenheimer approximation) for a state in the electronic continuum. This equation for two electrons in the screened field of two nuclei (A and B) with charges Z_A and Z_B reads

$$[\hat{H}(\{\mathbf{r}\};R,\{\boldsymbol{\lambda}\})-E]\Psi(\{\boldsymbol{r}\};R,\{\boldsymbol{\lambda}\})=0, \tag{1}$$

with the Hamiltonian given by

$$\hat{H}(\{\mathbf{r}\};R,\{\boldsymbol{\lambda}\})=\sum_{i=1,2}\hat{h}(\mathbf{r}_i;R,\lambda_p)+\frac{e^{-\lambda_e r_{12}}}{r_{12}}+\frac{Z_A Z_B e^{-\lambda_N R_{AB}}}{R_{AB}}, \tag{2}$$

where $\{\boldsymbol{r}\}$ compactly indicates the coordinates for the two electrons, i.e., $\{\mathbf{r}_1,\mathbf{r}_2\}$, and similarly $\{\boldsymbol{\lambda}\}$ is the set $\{\lambda_p,\lambda_e,\lambda_N\}$ of electron-nuclei, electron-electron, and nucleus-nucleus screening parameters, respectively. Also, r_{12} and R_{AB} correspond to the interelectronic and internuclear distances, respectively. Each one-electron Hamiltonian is given by

$$\hat{h}(\mathbf{r}_i;R,\lambda_p)=-\frac{1}{2}\boldsymbol{\nabla}^2_{\mathbf{r}_i}-\frac{Z_A e^{-\lambda_p r_{iA}}}{r_{iA}}-\frac{Z_B e^{-\lambda_p r_{iB}}}{r_{iB}}, \tag{3}$$

for $i=1,2$, where r_{iA} and r_{iB} stand for the electron-nucleus distances. The latter Hamiltonian is also associated to an eigensystem for the screened molecular orbitals, i.e.,

$$[\hat{h}(\mathbf{r}_i;R,\lambda_p)-\epsilon_k]\psi_k(\mathbf{r}_i;R,\lambda_p)=0. \tag{4}$$

The one-electron two-center screened Coulomb problem represented by Eq. (4) has been comprehensively studied by us in a recent work [5]. Our approach to solve that problem was based on a partial-wave expansion in terms of confocal elliptic coordinates, naturally adapted to solve two-center problems. However, to solve the two-electron two-center screened Coulomb problem for the electronic continuum using confocal elliptic coordinates is rather complicated, although feasible for bound and quasibound states [11,12]. It has been shown that one-center spherical partial-wave expansions are better suited for the description of the molecular electronic continuum [10,13]. Since we are interested here in resonances immersed in the electronic continuum, we adopt this approach.

The nuclear repulsion term in Eq. (2) will be removed in the following since here we are only concerned with the electronic structure. Nevertheless, it may play a significant role when considering the nuclear motion due to the removal of the Coulomb long-range interaction (see, for instance, our work on screened H_2^+ [5]). In principle, the screening parameter λ should be physically different for the three types of Coulomb interaction terms (electron-nucleus λ_p, electron-electron λ_e, and among nuclei λ_N) due to the different mobility of the charged particles involved. Therefore, we expect $\lambda_p > \lambda_e$ because, due to their different masses, nuclei have longer reaction times than electrons to induce screening.

To unveil the influence of screening on resonances in two-electron diatomic molecules, one must be aware in advance that the resonance autoionization process is purely due to electron correlation, so that the electron-electron repulsion term in the Hamiltonian plays a fundamental role. Screening enters in two levels: first, the electron-nucleus screening (with λ_p) modifies the nature of the molecular orbitals that enter into the two-electron configuration interaction; second, the screened interelectronic term (with λ_e) is evaluated not only to obtain electron-correlated resonance and continuum two-electron wave functions (both resonance states and the underlying continuum are treated on equal footing with respect

to screening), but also to obtain the resonance widths by using Fermi's golden rule as shown below.

A. One-center screened molecular orbitals

We make use of one-center partial-wave expanded molecular orbitals $\psi(\mathbf{r})$ of the form [13]

$$\psi^{m\pi}(r,\theta,\phi) = \sum_{\ell} \frac{u_\ell(r)}{r} Y_\ell^m(\theta,\phi), \tag{5}$$

where the reduced radial part u_ℓ is expanded using N_B B-splines with polynomial order k, i.e., $u_\ell(r) = \sum_{i=1}^{N_B} c_{i,\ell} B_i^k(r)$. For homonuclear molecules, $Z_A = Z_B$, and for nuclear masses $M_A = M_B$, the symmetry with respect to the inversion center operator $\hat{i}$ classifies molecular orbitals as gerade with $\pi = g$ (ungerade with $\pi = u$), so that only partial waves with even (odd) values of angular momentum ℓ contribute to the expansion. Molecular orbitals for different values of $\lambda = |m|$ ($\lambda = 0,1,2\ldots$ correspond to $\sigma,\pi,\delta\ldots$, respectively) are computed separately. B-splines are built within an electronic box in the interval $[0,r_{\max}]$ satisfying the boundary conditions by ensuring $B_i^k(0) = 0$ and $B_i^k(r_{\max}) = 0\ \forall i$. For a detailed discussion of the properties and applications of B-splines the reader is referred to Ref. [13]. The projection of Eq. (4) on this basis set transforms its solution into an algebraic eigenvalue form $(\mathbf{T}+\mathbf{V})\mathbf{C} = E\mathbf{S}\mathbf{C}$. The matrix elements of the overlap $\mathbf{S}$ and the kinetic operator $\mathbf{T}$,

$$S_{i\ell,j\ell'} = \delta_{\ell,\ell'} \int_0^{r_{\max}} dr\ B_i^k(r) B_j^k(r) \tag{6}$$

$$T_{i\ell,j\ell'} = \delta_{\ell,\ell'} \frac{1}{2}\Bigg[\int_0^{r_{\max}} dr\ \partial_r B_i^k(r) \partial_r B_j^k(r) + \ell'(\ell'+1) \int_0^{r_{\max}} dr\ \frac{B_i^k(r) B_j^k(r)}{r^2} \Bigg], \tag{7}$$

are independent of the screening parameter λ and block-diagonal in angular momentum. These radial integrals are evaluated very efficiently using Gaussian quadratures [13].

To calculate the nuclear attraction potential we make use of the expansion (see Appendix A) [14]

$$\frac{e^{-\lambda|\mathbf{r}-\mathbf{r}'|}}{|\mathbf{r}-\mathbf{r}'|} = \sum_{\ell=0}^{\infty} f_\ell\big(r,r';\lambda\big) P_\ell(\hat{\mathbf{r}}\cdot\hat{\mathbf{r}}'), \tag{8}$$

with

$$f_\ell(r,r';\lambda) = \lambda \frac{2}{\pi}[\ell] i_\ell(\lambda r_<) k_\ell(\lambda r_>), \tag{9}$$

where $i_\ell(x)$ and $k_\ell(x)$ are the modified spherical Bessel functions of the first and second kind, respectively, and $P_\ell(x)$ is a Legendre polynomial, $r_< = \min(r,r')$, and $r_> = \max(r,r')$. Throughout this work we use the contracted notation $[\ell] = (2\ell+1)$, whenever an angular momentum label is inside the square brackets. Although formally this screened expression for f_ℓ reduces identically to the well-known unscreened one $\frac{r_<^\ell}{r_>^{\ell+1}}$ in the limit $\lambda \to 0$, it is not appropriate for numerical evaluation of the unscreened case since it may lead to overflows because $k_\ell(x\to 0) \to \infty$. We have evaluated successfully and accurately the function $f_\ell(r,r';\lambda)$ for a large array of (r,r') quadrature points within the box $[0,r_{\max}]$, for different screening parameters λ, and for several values of the angular momentum ℓ. It is definitely a well-behaved function for our computational tasks, and thus we adopt this expression to solve our problem. The internuclear distance R is oriented along the z axis, and the origin of coordinates is located at the nuclear center of mass, with nucleus A on the negative z axis and nucleus B on the positive side. Thus the electron with position vector $\mathbf{r}$ feels the nucleus A with screened charge $Z_A e^{-\lambda_p|\mathbf{r}+\frac{M_B}{M_A+M_B}R\hat{\mathbf{z}}|}$ and nucleus B with a charge $Z_B e^{-\lambda_p|\mathbf{r}-\frac{M_A}{M_A+M_B}R\hat{\mathbf{z}}|}$. In the present work we deal with H_2, so that $Z_A = Z_B = 1$ and $M_A = M_B$ and thus the nuclear center of mass coincides with the geometrical midpoint.

Consequently, the nuclear attraction potential $\mathbf{V}$ has matrix elements in the form

$$V_{i\ell,j\ell'} = \int d\mathbf{r} \frac{B_i^k(r)}{r} Y_\ell^{m*}(\Omega) \frac{e^{-\lambda_p|\mathbf{r}\pm\frac{R}{2}\hat{\mathbf{z}}|}}{\left|\mathbf{r}\pm\frac{R}{2}\hat{\mathbf{z}}\right|} \frac{B_j^k(r)}{r} Y_{\ell'}^m(\Omega) = \sum_{\ell''=0}^{\infty} I^{\rm ang}_{\ell,\ell'',\ell'} I^{\rm rad}_{i,\ell'',j}, \tag{10}$$

where the plus (minus) sign is taken for the proton on the negative (positive) z axis. The angular integral $I^{\rm ang}_{\ell,\ell'',\ell'}$ in Eq. (10) has the closed form

$$I^{\rm ang}_{\ell,\ell'',\ell'} = \int d\Omega Y_\ell^{m*}(\Omega) P_{\ell''}(\pm\cos\theta) Y_{\ell'}^m(\Omega) = (\pm 1)^{\ell''}(-1)^m [\ell,\ell']^{1/2} \begin{pmatrix} \ell & \ell'' & \ell' \\ 0 & 0 & 0 \end{pmatrix} \begin{pmatrix} \ell & \ell'' & \ell' \\ -m & 0 & m \end{pmatrix}, \tag{11}$$

where we have used the shortened notation $[k_1,k_2,\ldots] = (2k_1+1)(2k_2+1)\ldots$ From Eq. (11) it is clear that the length of the partial-wave expansion for the molecular orbital in Eq. (5) determines the representation of the nuclear potential. The matrix $\mathbf{V}$ is not block-diagonal in angular momenta, but from our analysis of the behavior of the f_ℓ function the matrix elements closer to the diagonal $\ell = \ell'$ are the ones more affected by the screening. The radial integral $I^{\rm rad}_{i,\ell'',j}$ in Eq. (10) can be evaluated by splitting the integral in the *symmetric* form

$$I^{\rm rad}_{i,\ell'',j} = \int_0^{r_{\max}} dr\, B_i(r) f_{\ell''}\big(r,R/2;\lambda_p\big) B_j(r) = k'_\ell(\lambda_p,R/2) \int_0^{R/2} dr\, B_i(r) i'_\ell(\lambda_p,r) B_j(r) + i'_\ell(\lambda_p,R/2) \int_{R/2}^{r_{\max}} dr\, B_i(r) k'_\ell(\lambda_p,r) B_j(r), \tag{12}$$

where we have dropped the index k for the polynomial order of B-splines, and we have defined the auxiliary functions $i'_\ell(\lambda,r) = i_\ell(\lambda r)$ and $k'_\ell(\lambda,r) = \frac{2}{\pi}\lambda[\ell]k_\ell(\lambda r)$. The integrals included in Eq. (12) can be performed numerically with the same quadratures used for Eq. (7), since the evaluation of the modified spherical Bessel functions $i_\ell(x)$ and $k_\ell(x)$ [which are real valued in contrast with other known alternative expansions of Eq. (8) (see Appendix A)] can be obtained using standard numerical libraries [15] at any required real-valued grid point.

B. The two-electron problem with screening: Feshbach method

In the present work we deal with H_2, a homonuclear diatomic molecule, that belongs to the continuous point group $\mathcal{D}_{\infty h}$. Accordingly, the eigenstates Ψ (for bound, resonance and continuum states) of Eq. (1) are classified according to spin, inversion parity, and an irreducible representation of $\mathcal{D}_{\infty h}$, i.e., we use the notation $^{2S+1}\Lambda_\pi$, where S corresponds to spin (singlet $S=0$ or triplet $S=1$), $\Lambda = |M_L|$ takes the values 0 (Σ), 1 (Π), 2 (Δ), ... and for the inversion parity, states can be gerade ($\pi = \mathrm{g}$) or ungerade ($\pi = \mathrm{u}$). For Σ states, there exists also a distinction between eigenstates being symmetric (Σ^+) or antisymmetric (Σ^-) against a reflection through any plane containing the internuclear axis. Our present study will report only energies and widths of the lowest resonance with symmetry $^1\Sigma_g^+$ in H_2.

To compute resonance energies and widths we closely follow the $\mathcal{L}^2$ multichannel close-coupling method developed in [10,16], as adapted from the two-electron atomic context [17] (see also Ref. [13]). The method is inspired by the stationary Feshbach projection method, which has recently been applied by us to three-electron atoms [18] (in a complete form) and even to screened atomic helium using explicitly correlated coordinates [1]. Since the theory is explained in detail in the previous references we only give some guidelines. The total resonance wave function Ψ in Eq. (1) is separated into a boundlike part ($\mathcal{Q}$ half-space) and a scatteringlike part ($\mathcal{P}$ half-space) in the form $\Psi = \mathcal{Q}\Psi + \mathcal{P}\Psi$, where $\mathcal{Q}$ and $\mathcal{P}$ are projection operators satisfying completeness ($\mathcal{P}+\mathcal{Q}=1$), orthogonality ($\mathcal{P}\mathcal{Q}=0$), and idempotency ($\mathcal{P}^2=\mathcal{P}$ and $\mathcal{Q}^2=\mathcal{Q}$). The working equations derived from Eq. (1) with the molecular Hamiltonian (2) projected onto these half-spaces are

$$(\mathcal{Q}\hat{H}\mathcal{Q} - \mathcal{E}_s)\Phi_s = 0, \tag{13}$$

$$\mathcal{P}\big[\hat{H} + \hat{H}\mathcal{Q}G_{\mathcal{Q}}^{(s)}(E)\mathcal{Q}\hat{H} - E\big]\mathcal{P}\Psi_{\mu E}^{0-} = 0, \tag{14}$$

for a boundlike part $\Phi_s \equiv \mathcal{Q}\Psi$ of the resonance with energy $\mathcal{E}_s$ and for the *nonresonant* scatteringlike part $\mathcal{P}\Psi_{\mu E}^{0-}$ of the continuum at energy $E \approx \mathcal{E}_s$ satisfying incoming boundary conditions for the scattering channel μ. The energy-dependent operator $G_{\mathcal{Q}}^{(s)}(E)$ for the resonance Φ_s is explained below.

The molecular continuum has intrinsically a multichannel character. Each channel index μ in Eq. (14) is a contraction of labels, e.g., $\mu = \{\nu,\ell,\lambda,\pi,\sigma,S,M_S\}$, where ν collects the quantum numbers of the target (H_2^+ ion) state, ℓ is the angular momentum of the escaping electron, λ is the absolute value of the z component of the total angular momentum, π is the label for the inversion parity, σ the reflection symmetry with respect to a plane containing the internuclear axis, and S and M_S refer to total spin and its z projection, respectively. The autoionization width of a resonance with energy $\mathcal{E}_s$[1] is given by Fermi's golden rule:

$$\Gamma_s = \sum_\mu \Gamma_{s\mu} = 2\pi \sum_\mu \left|\langle \mathcal{P}\psi_{\mu E=\mathcal{E}_s}^{0-} \middle| \mathcal{P}H\mathcal{Q}|\Phi_s\rangle\right|^2, \tag{15}$$

where $\Gamma_{s\mu}$ is the partial width contribution from channel μ.

The solution of the boundlike equation (13) can be obtained using the configuration interaction (CI) method, in terms of symmetry-adapted products of molecular orbitals $\psi^{m\pi}$ previously computed from Eq. (4) in the form

$$\Phi_s = \sum_{i,j} c_{ij}\Theta\big[\psi_i^{m_i\pi_i}(\mathbf{r}_1)\psi_j^{m_j\pi_j}(\mathbf{r}_2)\big], \tag{16}$$

where the angular projections must satisfy $M_L = m_i + m_j$ and the total inversion symmetry is given by $\pi = \pi_i \times \pi_j$. Θ is the operator that performs the appropriate combinations to ensure the correct spin and reflection (for $\Sigma^\pm$ states) symmetries. For example, in the latter case, configurations of the type $[n_i\sigma_{g/u}(1),n_j\sigma_{g/u}(2)]$, $[n_i\pi_{g/u}(1),n_j\pi_{g/u}(2)]$, $[n_i\delta_{g/u}(1),n_j\delta_{g/u}(2)]$, etc., contribute to the $\Sigma_{g/u}^{\pm}$ symmetry. In this case $\Theta[\psi_i^{m_i\pi_i}(\mathbf{r}_1)\psi_j^{m_j\pi_j}(\mathbf{r}_2)]$ produces the following combinations:

$$\begin{aligned}&\tfrac{1}{2}\big\{\big[\psi_i^{m_i,\pi_i}(\mathbf{r}_1)\psi_j^{-m_j,\pi_j}(\mathbf{r}_2) \pm \psi_i^{-m_i,\pi_i}(\mathbf{r}_1)\psi_j^{m_j,\pi_j}(\mathbf{r}_2)\big]\\ &\pm\big[\psi_i^{m_i,\pi_i}(\mathbf{r}_2)\psi_j^{-m_j,\pi_j}(\mathbf{r}_1) \pm \psi_i^{-m_i,\pi_i}(\mathbf{r}_2)\psi_j^{m_j,\pi_j}(\mathbf{r}_1)\big]\big\},\end{aligned} \tag{17}$$

where the $\pm$'s inside the square brackets correspond to the reflection symmetry and the $\pm$ between squared brackets allows for the spin-adapted symmetry. As usual, in many practical applications of Feshbach-like methods in atoms and molecules, we do not calculate explicitly the projection operators $\mathcal{Q}$ and $\mathcal{P}$. For the boundlike part of resonant doubly excited states lying above the first ionization threshold and below the second one, the Hamiltonian is implicitly $\mathcal{Q}$-projected by excluding the $\psi_1^{0,g} \equiv 1\sigma_g$ molecular orbital from the configurations used in Eq. (16) (truncated diagonalization method), thus (i) avoiding a variational collapse to the ground state and producing the lowest eigenvalues for the doubly excited states, and (ii) guaranteeing orthogonality with the continuum $\mathcal{P}\Psi$ built using a static exchange approximation (as detailed below) with configurations of the form $[1\sigma_g(1),\epsilon\ell_i m_{\ell_i}(2)]$.

$G_{\mathcal{Q}}^{(s)}(E)$ in Eq. (14) is the Green operator (resolvent) $1/\mathcal{Q}(E-\hat{H})\mathcal{Q}$ for the $\mathcal{Q}$ half-space, but devoid of any contribution coming from the resonance state Φ_s, i.e., this Green operator expanded in the eigenstates of $\mathcal{Q}\hat{H}\mathcal{Q}$ reads $G_{\mathcal{Q}}^{(s)}(E) = \sum_{n\neq s} |\Phi_n\rangle\langle\Phi_n|/(E-\mathcal{E}_s)$.

The nonresonant equation (14) can be solved in its integral Lippmann-Schwinger form

$$\mathcal{P}\Psi_{\mu E}^{0-} = \chi_{\mu E}^0 + G_P^{(s)-}(E)V\chi_{\mu E}^0, \tag{18}$$

where $G_P^{(s)-}(E) = \mathrm{P}(\frac{1}{E-\mathcal{P}\hat{H}'\mathcal{P}}) + i\pi\delta(E-\mathcal{P}\hat{H}'\mathcal{P})$ is the Green function for the $\mathcal{P}$ half-space [$\hat{H}'$ indicates the full operator appearing in Eq. (14) and the P(x) symbol stands for the Cauchy principal value] using uncoupled continuum states (UCS) $\chi_{\mu E}^0$. The latter UCS states are eigenfunctions of the uncoupled molecular Hamiltonian for a given specific channel μ,

$$(P_\mu\hat{H}P_\mu - E)\chi_{\mu E}^0 = 0, \tag{19}$$

where P_μ is a projector for the channel μ. The solution of the Lippmann-Schwinger equation requires the UCS,

[1]Formally, the resonance energy is corrected by an energy shift such that $E_s = \mathcal{E}_s + \Delta_s$. This energy shift Δ_s is rather small for H_2, and it has not been included in this work.

the evaluation of the Green function $G_P^{(s)-}(E)$, and the interchannel coupling $V = \sum_{\mu\neq\mu'} P_\mu \hat{H} P_{\mu'}$. The UCS are built using a static exchange approximation of the form $\chi^0_{\mu E} = \Theta[\psi_\mu(\mathbf{r}_1,\hat{r}_2)\xi_{\mu E}(r_2)]$, where Θ is again the full operator that enforces symmetrization (antisymmetrization) for spin-singlet (triplet) and correct inversion and reflection parities. $\xi_{\mu E}$ is the radial wave function for the electron in the continuum, and ψ_μ is the channel function, a composition of the target state with the angular momentum of the ejected electron, coupled to provide the total correct symmetry of the channel. In practice, for instance, for the electronic continuum above the first ionization threshold H_2^+ ($1s\sigma_g$), our UCS wave functions are constructed using the CI method, but keeping the first electron fixed to the state $1s\sigma_g$ with the orbital $\psi_1^{0,g}$ (obtained as the lowest eigenstate from the eigensystem (4) for $|m| = 0$ and $\pi = g$). The second electron occupies quasiorbitals $\varphi_\ell^{m,\pi}$ characterized by a fixed angular momentum value ℓ. They are obtained by solving the same eigensystem (4) but only within a diagonal block with size $N_B \times N_B$ for a given ℓ. The CI method provides the Kronecker-δ normalized eigenstates

$$\tilde{\chi}^0_{\ell,n} = \Theta\left[\psi_1^{0,g}(\mathbf{r}_1)\sum_{j=1}^{N_B} c_{jn}\varphi_{\ell,j}^{m_j,\pi_j}(\mathbf{r}_2)\right], \tag{20}$$

with $n = 1,\ldots,N_B$ and c_{jn} is the CI expansion coefficient. These UCS states, properly Dirac-δ normalized with the density of states $\rho_\mu(E)$, are introduced in the Lippmann-Schwinger equation to produce the correct coupled continuum states for a discretized set of continuum energies $\{E_n\}$ that read

$$\mathcal{P}\psi^{0-}_{\mu E_n} = \rho_\mu^{1/2}(E_n)\left[\tilde{\chi}^0_{\mu n} + \sum_{\mu' n'}\sum_{\mu'' n''}\left\langle\tilde{\chi}^0_{\mu' n'}\middle|G_P^{(s)-}(E_n)\middle|\tilde{\chi}^0_{\mu'' n''}\right\rangle \times\left\langle\tilde{\chi}^0_{\mu'' n''}\middle|V\middle|\tilde{\chi}^0_{\mu n}\right\rangle\tilde{\chi}^0_{\mu' n'}\right]. \tag{21}$$

The computation of the Green's function matrix elements in (21) is reduced to an algebraic problem and it is described in detail in [17,19].

C. Two-electron integrals with screening

The computation of the CI matrix elements with the Hamiltonian (2) requires the efficient computation of the electron repulsion integrals $\langle\psi_a\psi_b|\frac{e^{-\lambda_e|\mathbf{r}-\mathbf{r}'|}}{|\mathbf{r}-\mathbf{r}'|}|\psi_c\psi_d\rangle$, which may be rewritten as

$$\sum_{\substack{\ell_a,\ell_b\\ \ell_c,\ell_d}}\int d\mathbf{r}\int d\mathbf{r}'\varrho_B(\mathbf{r})\frac{e^{-\lambda_e|\mathbf{r}-\mathbf{r}'|}}{|\mathbf{r}-\mathbf{r}'|}\varrho_A(\mathbf{r}'), \tag{22}$$

in terms of the electron distribution $\varrho_A(\mathbf{r}')$ expressed with one-center molecular orbitals

$$\varrho_A(\mathbf{r}') = \frac{u_{b,\ell_b}(r')u_{d,\ell_d}(r')}{r'^2}Y^{m_b^*}_{\ell_b}(\Omega')Y^{m_d}_{\ell_d}(\Omega'), \tag{23}$$

and the distribution $\varrho_B(\mathbf{r})$ (with an analogous expression with indices a and c). The rr' radial integral in (22) can be transformed into an r radial integral by introducing the potential function ϕ_A, e.g., $\int d\mathbf{r}\varrho_B(\mathbf{r})\phi_A(\mathbf{r};\lambda_e)$, with $\phi_A(\mathbf{r};\lambda_e) = \int d\mathbf{r}'\frac{e^{-\lambda_e|\mathbf{r}-\mathbf{r}'|}}{|\mathbf{r}-\mathbf{r}'|}\varrho_A(\mathbf{r}')$, a potential generated by the charge distribution ϱ_A. By introducing the expansion (8) in ϕ_A and making use of the addition theorem for $P_\ell(x)$ we obtain

$$\begin{aligned}\phi_A(\mathbf{r};\lambda_e) &= \int d\mathbf{r}'\sum_{\ell,m}\frac{4\pi}{[\ell]}f_\ell(r,r',\lambda_e)Y_\ell^m(\Omega)Y_\ell^{m*}(\Omega')\varrho_A(\mathbf{r}'),\\ &= \sum_{\ell,m}\frac{4\pi}{[\ell]}\frac{q_\ell^m(r;\lambda_e)}{r}Y_\ell^m(\Omega),\end{aligned} \tag{24}$$

where we have defined the multipole coefficients $q_\ell^m = y_\ell(r;\lambda_e)\cdot I^m_{\rm ang}$ [using also Eq. (23)], which contains

$$y_\ell(r;\lambda_e) = r\int dr' f_\ell(r,r';\lambda_e)\rho_A(r') \tag{25}$$

as the *auxiliary function*, with $\rho_A(r') = u_{b,\ell_b}(r')u_{d,\ell_d}(r')$ [similarly, $\rho_B(r) = u_{a,\ell_a}(r)u_{c,\ell_c}(r)$], and the Gaunt angular integral for spherical harmonics

$$I^m_{\rm ang} = \int d\Omega' Y_\ell^{m*}(\Omega')Y_{\ell_b}^{m_b*}(\Omega')Y_{\ell_d}^{m_d}(\Omega'). \tag{26}$$

The potential ϕ_A satisfies the screened Poisson equation

$$\left[\nabla^2 - \lambda_e^2\right]\phi_A(\mathbf{r};\lambda_e) = -4\pi\varrho_A(\mathbf{r}) \tag{27}$$

for the charge distribution ϱ_A. By replacing the multipolar expansions (24) for the potential and (23) for the charge distribution, we easily arrive at the radial screened Poisson equation[2]

$$\left[d_{r,r} - \frac{\ell(\ell+1)}{r^2} - \lambda_e^2\right]y_\ell(r;\lambda_e) = -[\ell]\frac{\rho_A(r)}{r}. \tag{28}$$

Once this radial differential equation is obtained, we solve it subject to the use of B-spline basis functions for the expansion and within an electronic radial box $[0,r_{\rm max}]$. Here we follow a procedure outlined in [9] for the pure Coulomb case and adapted here for the screened case. A solution for Eq. (28) is proposed in the form

$$y_\ell(r;\lambda_e) = y_\ell^{(0)}(r;\lambda_e) + \tilde{y}_\ell(r;\lambda_e), \tag{29}$$

such that $y_\ell^{(0)}$ and $\tilde{y}_\ell$ correspond to the particular and to the homogeneous solutions, respectively, of the second-order differential equation (28), subject to the boundary conditions of the radial box $[0,r_{\rm max}]$, namely,

$$y_\ell(0;\lambda_e) = y_\ell^{(0)}(0;\lambda_e) = \tilde{y}_\ell(0;\lambda_e) = y_\ell^{(0)}(r_{\rm max};\lambda_e) = 0 \tag{30}$$

and

$$\begin{aligned}y_\ell(r_{\rm max};\lambda_e) &= \tilde{y}_\ell(r_{\rm max};\lambda_e)\\ &= r_{\rm max}\int_0^{r_{\rm max}} dr' f_\ell(r_{\rm max},r';\lambda_e)\rho_A(r').\end{aligned} \tag{31}$$

The particular solution $y_\ell^{(0)}$ is determined by expanding the solution of Eq. (28) on the same B-spline basis $\{B_i^k\}$ already

[2]An alternative and interesting derivation for the radial screened Poisson equation is given in Appendix B.

used in Sec. II A that satisfies the previously stated boundary conditions, i.e.,

$$y_\ell^{(0)}(r;\lambda_e) = \sum_i C_i B_i^k(r). \tag{32}$$

Now, by projecting with $\int_0^{r_{\max}} B_j^k(r)$ one arrives to a corresponding matrix equation

$$\sum_i T_{ji}^{\ell,\lambda_e} C_i = [\ell] U_j^A, \tag{33}$$

where

$$T_{ji}^{\ell,\lambda_e} = -\int_0^{r_{\max}} B_j^k(r)\left(d_{r,r} - \frac{\ell(\ell+1)}{r^2} - \lambda_e^2\right) B_i^k(r) dr, \tag{34}$$

and

$$U_j^A = \int_0^{r_{\max}} B_j^k(r) \frac{1}{r} \rho_A(r) dr. \tag{35}$$

Consequently, the expansion coefficients are found to be

$$C_i = [\ell] \sum_{j=1} \left[T_{ij}^{\ell,\lambda_e}\right]^{-1} U_j^A. \tag{36}$$

The homogeneous differential equation for the screened Poisson equation

$$\left[d_{r,r} - \frac{l(l+1)}{r^2} - \lambda_e^2\right] \tilde{y}_l(r;\lambda_e) = 0 \tag{37}$$

can be readily obtained from the differential equation $[z^2 d_{z,z} + 2z d_z - \ell(\ell+1) - z^2] w(z) = 0$, which is satisfied by the modified spherical Bessel functions $i_\ell(z)$ and $k_\ell(z)$ [14], if we define $w(z) = v(z)/z$ and use the change of variables $z = \lambda r$ for $v(\lambda r)$. Thus the particular solution can be written as

$$\tilde{y}_\ell(r;\lambda_e) = A\lambda_e r i_\ell(\lambda_e r) + B\lambda_e r k_\ell(\lambda_e r). \tag{38}$$

The boundary conditions [Eqs. (30) and (31)] imply that $B = 0$ and that $A = y_\ell(r_{\max};\lambda_e)/[\lambda_e r_{\max} i_\ell(\lambda_e r_{\max})]$, so that the homogeneous solution is given by

$$\tilde{y}_\ell(r;\lambda_e) = \frac{2}{\pi}[\ell] \frac{k_\ell(\lambda_e r_{\max}) i_\ell(\lambda_e r) \lambda_e r}{i_\ell(\lambda_e r_{\max})} \times \int_0^{r_{\max}} dr' i_\ell(\lambda_e r') \rho_A(r'). \tag{39}$$

With the full solution for $y_\ell(r;\lambda_e)$, back substitution in the two-electron integral $\int d\mathbf{r} \varrho_B(\mathbf{r}) \phi_A(\mathbf{r},\lambda_e)$ yields a final expression for the bielectronic radial integral

$$I_r = \lambda_e \frac{2}{\pi}[\ell] \int_0^{r_{\max}} dr \int_0^{r_{\max}} dr' \rho_B(r)\, i_\ell(\lambda_e r_<) k_\ell(\lambda_e r_>) \rho_A(r'), \tag{40}$$

of the form

$$I_r = \sum_i C_i U_i^B + \lambda_e \frac{2}{\pi}[\ell] \frac{k_\ell(\lambda_e r_{\max})}{i_\ell(\lambda_e r_{\max})} Q_\ell^B Q_\ell^A, \tag{41}$$

where

$$U_i^B = \int_0^{r_{\max}} B_i^k(r) \frac{1}{r} \rho_B(r) dr, \tag{42}$$

and

$$Q_\ell^A = \int_0^{r_{\max}} dr\, i_\ell(\lambda_e r) \rho_A(r), \tag{43}$$

$$Q_\ell^B = \int_0^{r_{\max}} dr\, i_\ell(\lambda_e r) \rho_B(r). \tag{44}$$

These algorithms were included in our suite of CI codes to compute both resonance and continuum states. To check the correctness of our integration algorithm we have computed some tabulated two-electron direct integrals $F^k(n\ell,n'\ell')$ [20] with $k = 0,2,4,6$, and $n\ell$ and/or $n'\ell' = 1s,2s,2p,3d,4s,4d,4f$ for the unscreened case by using $\lambda_e = 10^{-9}$ obtaining 9–10 correct figures. For the screened case we have compared the results from our screened Poisson equation method with those obtained with integration by double quadrature, comparing well with eight to nine significant digits, for $\lambda_e = 0.1$ a.u. Of course, the procedure to evaluate two-electron integrals in terms of the Poisson equation speeds up our CI computations by orders of magnitude compared to using a crude 2D quadrature formula.

III. RESULTS

First we have computed one-electron molecular orbitals using a B-spline basis set, following the guidelines of Sec. II A. The radial part of the H_2^+ orbitals was described using 180 B-splines of degree $k = 8$ on a linear breakpoint sequence inside an electronic box of size $r_{\max} = 60$ a.u., and for the angular part the maximum angular momentum used for each inversion symmetry (gerade or ungerade) was $\ell_{\max} = 16$. The integrals with polynomial integrands were calculated with exact quadratures and the rest using 12 quadrature points.

We calculate the lowest resonances of symmetry $^1\Sigma_g^+$, located below the second ionization threshold. The 236 configurations used in $\mathcal{Q}$ space for the boundlike part of the resonant state, of the form $[n_1\lambda_\pi^{\pm m}(1); n_2\lambda_\pi^{\mp m}(2)]$, are summarized in Table I. We remark here that throughout the text we make use of the familiar notation for unscreened (united atom) one-electron diatomic molecule orbitals to name screened orbitals, so that $1s\sigma_g \equiv 1\sigma_g$, $2s\sigma_g \equiv 2\sigma_g$, $2p\sigma_u \equiv 1\sigma_u$, $3p\sigma_u \equiv 2\sigma_u$, etc.

For the complementary $\mathcal{P}$ space, we first compute the UCS for which we have used configurations in the form

TABLE I. Configurations used to calculate energies and wave functions for the doubly excited states of symmetry $^1\Sigma_g^+$ in screened H_2. Here n_i indicates the index of the molecular orbital (ordered in ascending energy). There are 236 configurations in total.

$\lambda_\pi^{\pm m}(1)$	$\lambda_\pi^{\mp m}(2)$	n_1	n_2
σ_u	σ_u	1	1–70
π_u^+	π_u^-	1	1–70
σ_g	σ_g	2	2–35
σ_u	σ_u	2	2–18
σ_g	σ_g	3	3–18
π_g^+	π_g^-	1	1–10
δ_g^+	δ_g^-	1	1–10
π_u^+	π_u^-	2	2–10

TABLE II. Comparison of resonance energies and widths between the lowest resonance of symmetry $^1\Sigma_g^+$ in H_2 for the internuclear distance $R = 0.01$ a.u. and the lowest resonance of symmetry ^1S_e in He [1].

	$\lambda_p = \lambda_e = 0$		$\lambda_p = \lambda_e = 0.2$ a.u.	
State	$\mathcal{E}_s$ (a.u.)	Γ_s (a.u.)	$\mathcal{E}_s$ (a.u.)	Γ_s (a.u.)
H_2 $1^1\Sigma_g^+$	–0.77615	5.74×10^{-3}	–0.30772	4.63×10^{-3}
He 1^1S^e	–0.77794	4.53×10^{-3}	–0.31114	3.13×10^{-3}

$[1s\sigma_g, n\sigma_g^\ell]$, where $n\sigma_g^\ell$ denotes the nth molecular orbital (ordered in ascending energy) obtained from the solution of the Schrödinger equation for screened H_2^+ using only a single value of angular momentum ℓ in the basis. We have computed UCS with angular momenta $\ell = 0,2,4,6$ by including the lowest 75 states $n = 1$–75 of σ_g^ℓ symmetry for each value ℓ.

To check our computational procedure for the molecular resonant states of H_2 under screened Coulomb potentials, we first compare our H_2 results with those obtained for screened He (united atom limit of H_2) using also a Feshbach formalism and an explicitly correlated atomic basis [1]. For that purpose we set the internuclear distance close to zero in our molecular code. The lowest resonance of $^1\Sigma_g^+$ symmetry in H_2 (with a leading configuration $[2s\sigma_g]^2$ at short internuclear distances) must correlate to the lowest resonance of $^1S^e$ in He (with a dominant configuration $[2s]^2$) when $R \to 0$. Table II shows the comparison of energies and widths of this lowest resonance for $R = 0.01$ a.u. and $\lambda_p = \lambda_e = 0$ and $\lambda_p = \lambda_e = 0.2$ a.u. The comparison is quite satisfactory, especially considering the unpaired precision of the results obtained in He because of using explicitly correlated bases and the sensitivity of the Auger widths to the details of the wave functions.

In the following we analyze the effect of introducing a different screening in the electron-nucleus (λ_p) and electron-electron (λ_e) Coulomb interactions. We will consider that the upper limit of electron screening is given by the nuclear screening parameter, so that $0 \leqslant \lambda_e \leqslant \lambda_p$, and we take the boundary values $\lambda_e = 0$ and $\lambda_e = \lambda_p$ for the calculation of the lowest resonance $\mathcal{Q}_1\,^1\Sigma_g^+$. This molecular resonant state, under pure Coulomb interactions, is embedded in the continuum between the first H_2^+ $(1s\sigma_g)$ and the second H_2^+ $(2p\sigma_u)$ ionization thresholds. The energies for H_2^+ states subject to screening have been calculated quite accurately with another separate code based on confocal elliptic coordinates [5]. At the internuclear distance $R \approx 2.7$ a.u. the resonance crosses the lower limit $1s\sigma_g$, thus losing its resonance character and becoming a Rydberg bound state (see Fig. 1). Screening changes the binding properties among particles, and in molecules this effect also depends upon the internuclear distance. To keep the character of the molecular resonance, we have limited the values of the screening parameters λ_e and λ_p so that the resonance always lies below the second *screened* ionization threshold. With unscreened electron-electron interaction ($\lambda_e = 0$), the limiting screening value for the electron-proton interaction is $\lambda_p = 0.11$ a.u., for which the resonance energy still remains below the upper ionization threshold H_2^+ $(2p\sigma_u)$ at any internuclear distance. It is worth noting here that higher resonances in the $\mathcal{Q}_1\,^1\Sigma_g^+$ series disappear. However,

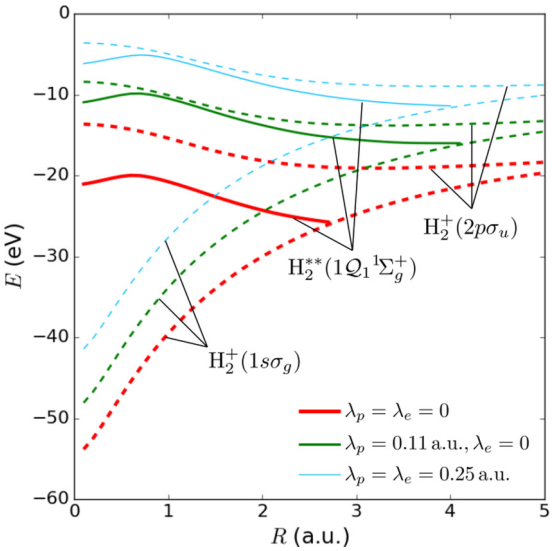

FIG. 1. Electronic energy of the lowest $\mathcal{Q}_1\,^1\Sigma_g^+$ doubly excited resonance state (solid lines) along with the first H_2^+ $(1s\sigma_g)$ and the second H_2^+ $(2p\sigma_u)$ ionization thresholds (dashed lines) as a function of internuclear distance for different values of λ_p and λ_e. Thick red lines correspond to the unscreened case, $\lambda_p = \lambda_e = 0$; green lines to electron-proton screening, $\lambda_p = 0.11$ a.u. and $\lambda_e = 0$ a.u.; and thin blue lines to the case when both electron-proton and electron-electron interactions are screened, with $\lambda_p = \lambda_e = 0.25$ a.u.

if screening is also introduced among electrons, this critical value increases up to $\lambda_p = \lambda_e = 0.25$ a.u.

Figure 1 shows the electronic energy of the lowest $\mathcal{Q}_1\,^1\Sigma_g^+$ resonance and of the lower $(1s\sigma_g)$ and upper $(2p\sigma_u)$ ionization thresholds for the different combinations of screening parameters mentioned previously: (i) $\lambda_p = \lambda_e = 0$, (ii) $\lambda_p = \lambda_e = 0.25$ a.u., and (iii) $\lambda_p = 0.11$ a.u. with $\lambda_e = 0$. It can be seen that the introduction of screening shifts all energies upwards by approximately a constant value independent of R and, as in the He case previously reported [1], the energy of the resonance moves up by a larger amount than the thresholds do. This can be easily understood from a Taylor expansion of the molecular potential up to first order in λ_p and λ_e,

$$V_{1e}(\lambda_p) = \sum_{A=1}^{N}\left(-\frac{e^{-\lambda_p r_{1A}}}{r_{1A}}\right) \approx \sum_{A=1}^{N}\left(-\frac{1}{r_{1A}} + \lambda_p\right) = V_{1e}(0) + N\lambda_p, \qquad (45)$$

which shows that for one-electron molecular systems the potential is shifted by a quantity $N\lambda_p$, where N is the number of nuclei in the molecule, while for two-electron systems, the Taylor expansion

$$V_{2e}(\lambda_p,\lambda_e) = \sum_{A=1}^{N}\left(-\frac{e^{-\lambda_p r_{1A}}}{r_{1A}} - \frac{e^{-\lambda_p r_{2A}}}{r_{2A}}\right) + \frac{e^{-\lambda_e r_{12}}}{r_{12}} \approx \sum_{A=1}^{N}\left(-\frac{1}{r_{1A}} - \frac{1}{r_{2A}} + 2\lambda_p\right) + \frac{1}{r_{12}} - \lambda_e = V_{2e}(0,0) + 2N\lambda_p - \lambda_e \qquad (46)$$

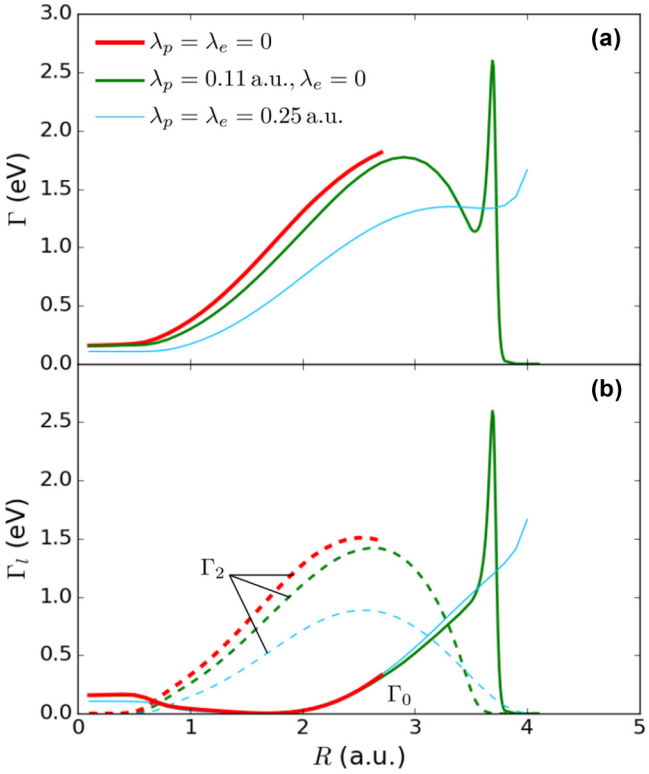

FIG. 2. Total width Γ (panel a, solid lines) and partial widths $\Gamma_{\ell=0}$ (solid lines) and $\Gamma_{\ell=2}$ (dashed lines) (panel b) of the lowest $Q_1\ ^1\Sigma_g^+$ resonance as a function of the internuclear distance for different values of λ_p and λ_e. Thick red lines correspond to the unscreened case, $\lambda_p = \lambda_e = 0$, green lines to the electron-proton screened case, with $\lambda_p = 0.11$ a.u. with $\lambda_e = 0$ a.u., and thin blue lines to electron-proton plus electron-electron screening, with $\lambda_p = \lambda_e = 0.25$ a.u. The partial widths $\Gamma_{\ell=4}$ and $\Gamma_{\ell=6}$ are approximately zero and are not shown here for the sake of clarity. Widths are plotted only up to the internuclear distance R at which the resonance energies plotted in Fig. 1 cross the lower threshold H_2^+ $(1s\sigma_g)$.

indicates that the potential is shifted by $2N\lambda_p - \lambda_e$. In our present case $N = 2$, and the energies of the ionization thresholds and of the resonance are shifted up by approximately $2\lambda_p$ and $4\lambda_p - \lambda_e$, respectively. In conclusion, two-electron energies increase faster than one-electron energies. Equations (45) and (46) explain the main features[3] of Fig. 1, namely, (i) the energies are shifted by an amount approximately independent of R, and (ii) the energy spacing between the quasiparallel curves depend upon the number of electrons and the two screening parameters λ_p and λ_e.

Although the screening effects on energy shifts are similar to the atomic case [1], in molecular resonances it may have implications on their nuclear dynamics because the uneven increase of the energies for the resonance and the ionization thresholds lead to resonance states that eventually survive for considerably larger internuclear distances (see Fig. 1). Furthermore, as explained below, it also has important implications on the resonance autoionization widths.

Figure 2 shows the total and partial widths of the lowest resonance as a function of the internuclear distance. Although we used even partial waves up to $\ell = 6$ for the continuum, the contribution of partial widths $\Gamma_{\ell=4}$ and $\Gamma_{\ell=6}$ (we use here ℓ to shorten the notation for channel μ) to the total width is very small and therefore they are not shown in Fig. 2. In the region of internuclear distances $0.7 \leqslant R \leqslant 2.7$ a.u. the partial width $\Gamma_{\ell=2}$ dominates. If only the electron-proton interaction is screened, the width is barely reduced in comparison with the unscreened case. However, when both electron-proton and electron-electron interactions are screened, the width is considerably reduced. This is because the electron-electron interaction is mainly responsible for the bound-to-continuum transitions and, consequently, its reduction due to screening causes a similar effect in the width.[4] At $R \approx 2.7$ a.u. the unscreened resonance encounters the lower threshold and, beyond that, only the resonances under screening conditions survive.

Beyond $R = 2.7$ a.u. we can see how, in both cases of screening under study, $\Gamma_{\ell=2}$ reaches its maximum and then decreases to zero while $\Gamma_{\ell=0}$ increases and becomes dominant. Moreover, in the case where only the electron-proton interaction is screened, $\Gamma_{\ell=0}$ displays a prominent peak in the region $3.6 \leqslant R \leqslant 3.8$ a.u., after which it goes to zero and remains so until it reaches the lower threshold at $R = 4.2$ a.u. In the case where both electron-proton and electron-electron interactions are screened, the total width is reduced overall but increases monotonically with increasing R, with the exception of a small plateau due to the combined effect of the decrease of partial width $\Gamma_{\ell=2}$ and the increase of $\Gamma_{\ell=0}$. It is worth noting that the modification of the electron-electron interaction by screening allows us to partially uncover the nature of molecular resonances beyond the internuclear distance at which the resonance dissappears in the pure Coulomb case.

Figure 3 shows the weights $[|c_{ij}|^2$ in Eq. (16)] of the three most important CI configurations present in the lowest resonance $\mathcal{Q}_1\ ^1\Sigma_g^+$. Although the orbitals used in the CI method come from the solution of the screened H_2^+ problem and therefore depend on λ_p, the screened orbitals with the lowest energies (and with higher CI weights) remain more or less similar to the unscreened ones, and the comparison of CI weights under different screening conditions is still meaningful. In addition to the already known change of character from the dominant configuration $[2s\sigma_g]^2$ to the $[2p\sigma_u]^2$ one at $R \approx 0.6$ a.u. [10,16], Fig. 3 shows that screening does not substantially modify the weights of the configurations and hence cannot explain the behavior of the partial widths beyond $R \approx 2.7$ a.u. in Fig. 2. However, given that the configuration $[2p\sigma_u]^2$ clearly dominates for $R > 1.0$ a.u., we can assume that it will play the key role in explaining the behavior of the partial widths.

Thus we propose a simplified model aiming at explaining the qualitative behavior of the widths in Fig. 2 in terms of

[3]The exact values of the energies are, however, considerably different from those predicted by Eqs. (45) and (46), because for $r \approx 1$ a.u. and $\lambda \approx 0.1$ a.u., the product $\lambda r \not\ll 1$.

[4]However, this is not always the case. In the helium atom, the widths of some resonances increase along with the screening parameter within a certain region of λ_e values [1].

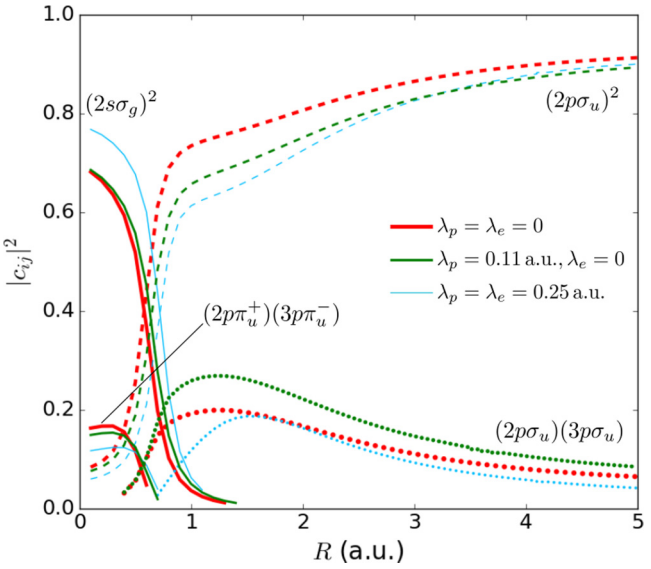

FIG. 3. Weights of the four most important CI configurations of the lowest resonance $\mathcal{Q}_1\ ^1\Sigma_g^+$ as a function of the internuclear distance. At short internuclear distances $(2s\sigma_g)^2$ dominates over $(2p\pi_u^+)(3p\pi_u^-)$ (both with solid lines). Above $R \approx 1$ a.u. the configuration $(2p\sigma_u)^2$ (dashed lines) dominates over $(2p\sigma_u)(3p\sigma_u)$ (dotted lines). Thick red lines correspond to the unscreened case, $\lambda_p = \lambda_e = 0$, green lines to the electron-proton screening, with $\lambda_p = 0.11$ a.u. and $\lambda_e = 0$, and thin blue lines to electron-proton plus electron-electron screening, with $\lambda_p = \lambda_e = 0.25$ a.u.

the radial parts of the $2p\sigma_u$ orbital and of the main UCS involved. The partial width for the decay into channel μ can be approximately written

$$\Gamma_\mu = 2\pi \left| \langle \psi_{\mu E_n} | \frac{e^{-\lambda_e r_{12}}}{r_{12}} | \Phi_s \rangle \right|^2 \approx 2\pi \left| \langle \chi_{\mu E_n} | \frac{e^{-\lambda_e r_{12}}}{r_{12}} | \Phi_s \rangle \right|^2, \tag{47}$$

where our first approximation has been to neglect the contribution of interchannel coupling $\sum_{\mu' \neq \mu} \langle \chi_{\mu' E_n} | \frac{e^{-\lambda_e r_{12}}}{r_{12}} | \Phi_s \rangle$ to the partial width from the continuum wave function (18). The integral inside Eq. (47) can be further approximated by retaining only the dominant configuration for the resonance, i.e.,

$$\left\langle 1s\sigma_g, \xi_{\mu E_n} Y_l^m \middle| \frac{e^{-\lambda_e r_{12}}}{r_{12}} | 2p\sigma_u, 2p\sigma_u \right\rangle = \int d\mathbf{r} \varrho_A(\mathbf{r}) f(\mathbf{r}), \tag{48}$$

where $f(\mathbf{r}) = \int d\mathbf{r}' \frac{e^{-\lambda_e r_{12}}}{r_{12}} \varrho_B(\mathbf{r}')$, with $\varrho_A(\mathbf{r}) = 1s\sigma_g(\mathbf{r}) 2p\sigma_u(\mathbf{r})$ and $\varrho_B(\mathbf{r}) = \xi_{\mu E_n}(r) Y_l^m(\hat{\mathbf{r}}) 2p\sigma_u(\mathbf{r})$. Since $\varrho_A(\mathbf{r})$ is the product of the wave functions of two deeply bound states and thus it is not very much dependent on the interelectronic interaction, Eq. (48) suggests that the features in Fig. 2 must be encoded in the distribution $f(\mathbf{r})$. To find simple arguments, we can simplify the evaluation of the latter function $f(\mathbf{r})$ by fixing the vector $\mathbf{r}$ at the origin, i.e., $\mathbf{r} = 0$, for which the integral is simplified considerably,

$$f(0) = \int d^3\mathbf{r}' \frac{e^{-\lambda_e r'}}{r'} \varrho_B(\mathbf{r}') = \left[\int_0^\infty dr'\, r' e^{-\lambda_e r'} \rho_B(r') \right] I_a, \tag{49}$$

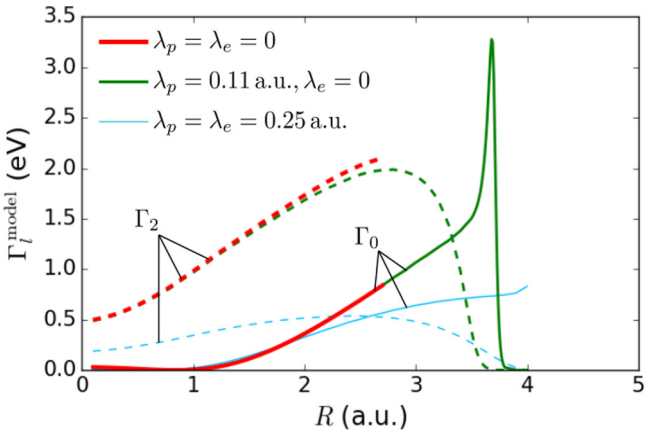

FIG. 4. Approximate partial widths $\Gamma_\ell^{\rm model}$ after Eq. (51), plotted as a function of the internuclear distance for partial waves $\ell = 0$ (solid lines) and $\ell = 2$ (dashed lines). Thick red lines correspond to the unscreened case, $\lambda_p = \lambda_e = 0$, green lines to the electron-proton screening, with $\lambda_p = 0.11$ a.u. and $\lambda_e = 0$, and thin blue lines to electron-proton plus electron-electron screening, with $\lambda_p = \lambda_e = 0.25$ a.u.

where $\rho_B(r)$ is the radial part[5] of $\varrho_B(\mathbf{r})$ and I_a is the angular integral. Note that $\varrho_B(\mathbf{r})$ is an odd function of $\mathbf{r}$ (ℓ is even in order to satisfy the overall gerade symmetry of the UCS), and thus $I_a = 0$, and consequently, $f(0) = 0$. However, the value of $f(\mathbf{r})$ at small distances from the origin (where I_a is different from zero) must also be approximately given by Eq. (49). In addition, the analysis of the coefficients of the $2p\sigma_u$ orbital shows that the angular distribution remains almost unchanged for $1 \leqslant R \leqslant 5$ a.u. so that the R dependence of $f(\mathbf{r})$ will be on the radial part of the integral, while the angular part I_a will remain mostly constant as R varies.

Having pinpointed the source of the (strongest) R dependence, the integral in Eq. (47) can be recast in the simplified form

$$\langle \chi_{\mu E_n} | \frac{e^{-\lambda_e r_{12}}}{r_{12}} | \phi_n \rangle \propto \int_0^\infty dr'\, r' e^{-\lambda_e r'} \rho_B(r'), \tag{50}$$

where the integration over $\mathbf{r}$ is assumed to add up to a constant approximately independent of R. Finally, inserting Eq. (50) in Eq. (47) we get

$$\Gamma_\mu^{\rm model} \propto \left| \int_0^\infty dr\, r e^{-\lambda_e r} \rho_B(r) \right|^2. \tag{51}$$

Figure 4 shows the right-hand side of the above equation as a function of internuclear distance. $\rho_B(r)$ is calculated as the product of $\xi_{\mu E_n}(r)$ times $2p\sigma_u(r)$, both evaluated along the z axis. The striking similarity between the *ab initio* partial widths plotted in Fig. 2 and the widths predicted using Eq. (51) and plotted in Fig. 4 is very remarkable, not only because of the number of approximations made to arrive at Eq. (51), but also because of its plain simplicity. Note that each curve in Fig. 4 is

[5]Actually, $2p\sigma_u(\mathbf{r})$ is not exactly separable into a radial and an angular part, but the latter is mostly $Y_1^0(\hat{\mathbf{r}})$, so it is approximately separable into a radial and an angular part.

correct only up to a constant (not necessarily the same constant for each curve). We obtain for the partial widths not only the leading behavior as a function of the internuclear distance, but also that their absolute values are close to the computed *ab initio* ones. Although this simplified model works well for the lowest $\mathcal{Q}_1\ ^1\Sigma_g^+$ resonance, its validity is uncertain for higher-lying resonances.

To finish the discussion on widths, we will address the sharp peak in Γ_0 (see Figs. 2 and 4), which appears in the case where only the proton-electron interactions are screened. In the static exchange approximation that we use to build the UCS, the effective Schrödinger equation for the wave function $\xi_{\mu E}$ of the continuum electron can be written as [21]

$$\left[-\frac{1}{2}\nabla_{\mathbf{r}}^2 + V(\mathbf{r})\right]\xi(\mathbf{r}) = \frac{k^2}{2}\xi(\mathbf{r}),$$

where the potential is

$$V(\mathbf{r})\xi(\mathbf{r}) = [V_Z(\mathbf{r}) + V_{1s\sigma_g}(\mathbf{r})]\xi(\mathbf{r}) + \int d^3r' K(\mathbf{r},\mathbf{r}')\xi(\mathbf{r}') \tag{52}$$

and whose components are

$$V_Z(\mathbf{r}) = -\frac{e^{-\lambda_p|\mathbf{r}-\mathbf{r}_A|}}{|\mathbf{r}-\mathbf{r}_A|} - \frac{e^{-\lambda_p|\mathbf{r}-\mathbf{r}_B|}}{|\mathbf{r}-\mathbf{r}_B|}, \tag{53}$$

$$V_{1s\sigma_g}(\mathbf{r}) = \int d^3\mathbf{r}' \frac{e^{-\lambda_e|\mathbf{r}-\mathbf{r}'|}}{|\mathbf{r}-\mathbf{r}'|}|1s\sigma_g(\mathbf{r}')|^2, \tag{54}$$

and

$$K(\mathbf{r},\mathbf{r}') = 1s\sigma_g^*(\mathbf{r})1s\sigma_g(\mathbf{r}')\left[\frac{e^{-\lambda_e|\mathbf{r}-\mathbf{r}'|}}{|\mathbf{r}-\mathbf{r}'|} - (E-k^2)\right], \tag{55}$$

where E corresponds to the total energy, k is the momentum of the continuum electron, V_Z is the potential due to the nuclei, $V_{1s\sigma_g}$ is the potential due to the $1s\sigma_g$ electron distribution, and K is the exchange potential. Figure 5 shows the direct potential $V_d(\mathbf{r}) = V_Z(\mathbf{r}) + V_{1s\sigma_g}(\mathbf{r})$ along the internuclear z axis for the different cases of screening. As can be seen, in the case where only the electron-proton interaction is screened, $V_d(\mathbf{r})$ displays a potential barrier. Like in the hydrogenic case [22] or in H_2^+ [5], the presence of this barrier leads to shape resonances. However, in the present case, the electron-electron interaction plays the role that the centrifugal potential does in the one-electron case, in the sense that even for $\ell = 0$ it decays slower (as $\sim 1/r$) than the nuclear potential (as $\sim -e^{-\lambda_p r}/r$). The reason we ignore $K(\mathbf{r},\mathbf{r}')$ in Fig. 5 is because it also decays as $\sim 1/r$ when only the electron-proton interaction is screened, and therefore it does not have a strong influence on the existence of a potential barrier. The height of the V_d barrier in Fig. 5 and the value of the continuum electron energy at the center of the peak located at $R = 3.7$ a.u. in Fig. 2 are both approximately 0.04 a.u. ($\sim$1 eV), which is in agreement with our reasoning. In conclusion, the peak present in Fig. 2 is very likely due to the partial decay of the Feshbach resonance into a temporary shape resonance when it approaches the lower ionization threshold, which, to our knowledge, is a metastable process not previously discussed in the literature.

Finally, it is worth pointing out that, although a previous study [23] of unscreened H_2 doubly excited states in the same region of internuclear distances has suggested that interaction with neighboring resonances could be important, the present model (which takes into account just a single resonance) shows that they are not responsible for the pronounced peak appearing in the autoionization width.

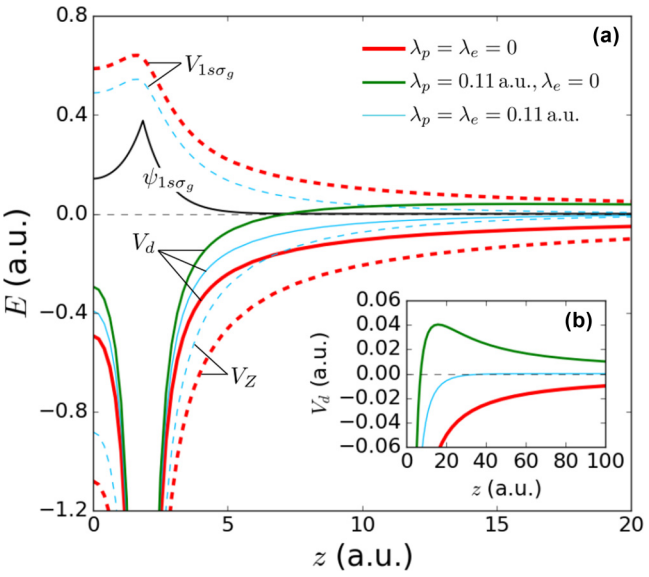

FIG. 5. (Panel a) Direct potential V_d and its components V_Z and $V_{1s\sigma_g}$ seen by the ionizing electron within the static exchange approximation at the internuclear distance $R = 3.7$ a.u. and as a function of z (along the internuclear axis). The black solid line corresponds to the $1s\sigma_g$ wave function. Solid lines: direct potential $V_d(\mathbf{r}) = V_Z(\mathbf{r}) + V_{1s\sigma_g}(\mathbf{r})$. Dashed lines: potential due to the H_2^+ ground state $V_{1s\sigma_g}(\mathbf{r})$ and potential generated by the nuclei $V_Z(\mathbf{r})$. Thick red lines correspond to the unscreened case, $\lambda_p = \lambda_e = 0$, green lines to the electron-proton screening, with $\lambda_p = 0.11$ a.u. and $\lambda_e = 0$, and thin blue lines to electron-proton plus electron-electron screening, with $\lambda_p = \lambda_e = 0.25$ a.u. (Inset, panel b) Detail of the direct potential V_d where a potential barrier appears only when the electron-proton interaction is screened. Note that V_Z only depends on λ_p and $V_{1s\sigma_g}$ only on λ_e, so that only two curves are drawn for both potentials.

IV. CONCLUSIONS

We have presented a general method to evaluate resonance parameters in diatomic molecules where Coulomb interactions are replaced by Yukawa-like ones. We have adopted one-center partial-wave expansions for both the bound and the continuum molecular orbitals with their radial parts described in terms of B-spline polynomials. The electron-nucleus interaction requires the evaluation of matrix elements involving modified spherical Bessel functions. The two-electron repulsion integrals are calculated through an auxiliary function that satisfies the screened Poisson equation subject to the boundary conditions provided by the electronic box. Details on the derivation of the radial screened Poisson equation have been given in the main text and Appendix B, where we have made use of a mathematical relation for the Bessel functions, yet unreported to our knowledge.

We have shown that screening of the electron-electron and electron-nucleus interactions plays a different role in

determining the metastability of H_2 molecular resonances. As expected, the main effect on the autoionization widths comes from the shielding of the electron-electron repulsion. However, screening effects can also lead to an interesting behavior: molecular resonances may extend their metastable character at internuclear distances larger than in the unscreened case, due to the different energy shifts of the two-electron resonance state and the one-electron ionization thresholds. This effect has allowed us to unveil the resonance structure beyond those critical internuclear distances where unscreened resonances cease to exist.

The variation of the autoionization widths with internuclear distance has also been analyzed by using a simplified model in which both the multichannel character of the electronic continuum and the multiconfigurational correlated nature of the resonance are neglected. In spite of its simplicity, the results of this model reproduce fairly well those obtained from *ab initio* calculations. Finally, we have also shown that, in the case of prevalent electron-proton screening, prominent peaks appearing in the autoionization widths at internuclear distances where the resonance approaches the lower ionization threshold are due to the presence of potential barriers in the effective screened Coulomb potential felt by the scattered electron. These barriers are eventually able to generate molecular shape resonances to which the lowest H_2 resonance can decay. Extension of this study to the full $\mathcal{Q}_1$ Rydberg series of resonances and to other molecules is under consideration for future work. We hope that the tools developed here and our analysis of these emerging physical effects in molecular resonances under screening conditions can be useful in future studies concerning, for example, molecular plasmas.

ACKNOWLEDGMENTS

We thank the GFIF-GFAM-UdeA computer cluster and CCC-UAM for generous allocation of computer time. This work was supported by an Advanced Grant of the European Research Council XCHEM (No. 290853), the European COST Action XLIC (Grant No. CM1204), and AEI-MINECO (Project No. FIS2016-77889-R). A.F.O.L. acknowledges financial support from EACEA through an Erasmus Mundus Scholarship. J.L.S.V. acknowledges financial support from Vicerrectoría de Investigación (Estrategia de Sostenibilidad) at Universidad de Antioquia and from Departamento Administrativo de Ciencia, Tecnología e Innovación (COLCIENCIAS, Colombia), through Grant No. 111565842968.

APPENDIX A: EXPANSION OF THE SCREENED COULOMB POTENTIAL

If in the well-known formula for an outgoing spherical wave $\frac{e^{ik|\mathbf{r}-\mathbf{r}'|}}{|\mathbf{r}-\mathbf{r}'|}$ [24] one sets $k = i\lambda$ with $\lambda \in \mathbb{R}$, the expansion for the Yukawa potential reads

$$\frac{e^{-\lambda|\mathbf{r}-\mathbf{r}'|}}{|\mathbf{r}-\mathbf{r}'|} = -\lambda \sum_{\ell=0}^{\infty} [\ell] j_\ell(i\lambda r_<) h_\ell^{(1)}(i\lambda r_>) P_\ell(\hat{\mathbf{r}}\cdot\hat{\mathbf{r}}') \quad \text{(A1)}$$

in terms of the spherical Bessel function $j_\ell(z)$ and the spherical Hankel function of the first kind $h_\ell^{(1)}(z)$, with $P_\ell(x)$ as the Legendre polynomials. Note that the arguments of the spherical functions are pure imaginary complex numbers. To keep the arguments in real space for computational purposes, we can rewrite (A1) in terms of the modified spherical Bessel functions of the first kind $i_\ell(x)$ and second kind $k_\ell(x)$, with $x \in \mathbb{R}$. For this we use the relations between the Bessel functions $\{J_\alpha, H_\alpha^{(1)}\}$, the modified Bessel functions $\{I_\alpha, K_\alpha\}$, the spherical Bessel functions $\{j_\ell, n_\ell\}$, and the modified spherical Bessel functions $\{i_\ell, k_\ell\}$ as follows [14,25]:

$$j_\ell(x) = \sqrt{\frac{\pi}{2x}} J_{\ell+\frac{1}{2}}(x); \text{ and } h_\ell^{(1)}(x) = \sqrt{\frac{\pi}{2x}} H_{\ell+\frac{1}{2}}^{(1)}(x), \quad \text{(A2)}$$

$$i_\ell(x) = \sqrt{\frac{\pi}{2x}} I_{\ell+\frac{1}{2}}(x); \text{ and } k_\ell(x) = \sqrt{\frac{\pi}{2x}} K_{\ell+\frac{1}{2}}(x), \quad \text{(A3)}$$

$$I_\alpha(x) = i^{-\alpha} J_\alpha(ix); \text{ and } K_\alpha(x) = \frac{\pi}{2} i^{\alpha+1} H_\alpha^{(1)}(ix). \quad \text{(A4)}$$

By employing these formulas we arrive at the useful relations

$$j_\ell(ix) = i^\ell i_\ell(x); \quad \text{and} \quad h_\ell^{(1)}(ix) = -\frac{2}{\pi i^\ell} k_\ell(x), \quad \text{(A5)}$$

that can be directly substituted in Eq. (A1) to give

$$\frac{e^{-\lambda|\mathbf{r}-\mathbf{r}'|}}{|\mathbf{r}-\mathbf{r}'|} = \lambda \frac{2}{\pi} \sum_{\ell=0}^{\infty} [\ell] i_\ell(\lambda r_<) k_\ell(\lambda r_>) P_\ell(\hat{\mathbf{r}}\cdot\hat{\mathbf{r}}'), \quad \text{(A6)}$$

which corresponds to the expansion used in this work.

APPENDIX B: ANOTHER EXCURSION TO THE RADIAL SCREENED POISSON EQUATION

For completeness, here we derive the radial screened Poisson equation otherwise. In this Appendix we drop the subscript e (electronic) in the screening parameter λ. The radial 2D integral (40) may be written in the form of a 1D integral

$$I_r = \int_0^{r_{\max}} dr \rho_B(r) \frac{1}{r} y_\ell(r;\lambda), \quad \text{(B1)}$$

where the auxiliary function $y_\ell(r;\lambda)$ (already defined in Eq. (25) and widely used in the atomic context [8]) contains two separate definite integrals

$$y_\ell(r;\lambda) = \lambda r C_\ell \Bigg[k_\ell(\lambda r) \int_0^r dr' i_\ell(\lambda r') \rho_A(r') + i_\ell(\lambda r) \int_r^{r_{\max}} dr' k_\ell(\lambda r') \rho_A(r') \Bigg], \quad \text{(B2)}$$

with $C_\ell = \frac{2}{\pi}[\ell]$. To find a second-order differential equation for y_ℓ we first find its first and second derivatives using the Leibnitz integral rule[6] and the recurrence relations for the

[6]The Leibnitz integral rule reads:

$$d_x \Bigg[\int_{g(x)}^{h(x)} f(t,x) dt \Bigg] = f(h(x),x) d_x h(x) - f(g(x),x) d_x g(x) + \int_{g(x)}^{h(x)} d_x f(t,x) dt.$$

modified spherical Bessel functions

$$i_{\ell-1}(x) - i_{\ell+1}(x) = \frac{[\ell]}{x} i_\ell(x), \tag{B3}$$

$$k_{\ell-1}(x) - k_{\ell+1}(x) = -\frac{[\ell]}{x} k_\ell(x), \tag{B4}$$

and their derivatives [14,25]

$$\ell i_{\ell-1}(x) + (\ell+1) i_{\ell+1}(x) = [\ell] d_x i_\ell(x), \tag{B5}$$

$$\ell k_{\ell-1}(x) + (\ell+1) k_{\ell+1}(x) = -[\ell] d_x k_\ell(x). \tag{B6}$$

The latter recurrences allow us to produce some alternative expressions for the derivatives,

$$\begin{aligned} d_x i_\ell(x) &= i_{\ell-1}(x) - \frac{\ell+1}{x} i_\ell(x) \\ &= i_{\ell+1}(x) + \frac{\ell}{x} i_\ell(x) \end{aligned} \tag{B7}$$

and

$$\begin{aligned} d_x k_\ell(x) &= -k_{\ell-1}(x) - \frac{\ell+1}{x} k_\ell(x) \\ &= -k_{\ell+1}(x) + \frac{\ell}{x} k_\ell(x). \end{aligned} \tag{B8}$$

We can use these expressions at convenience to calculate the second radial derivative of expression (B2) which, after a lengthy algebra, has the form

$$d_{r,r} y_\ell(r;\lambda) = C_\ell \{-\lambda[\ell] i_\ell(\lambda r) k_\ell(\lambda r) \rho_A(r) - \lambda^2 [i_\ell(\lambda r) k_{\ell-1}(\lambda r) + i_{\ell+1}(\lambda r) k_\ell(\lambda r)] r \rho_A(r)\} + \left[\frac{\ell(\ell+1)}{r^2} + \lambda^2\right] y_\ell(r;\lambda). \tag{B9}$$

We can rearrange the previous differential equation in the form of a Poisson-like equation as follows:

$$\left[d_{r,r} - \frac{\ell(\ell+1)}{r^2} - \lambda^2\right] y_\ell(r;\lambda) = -C_\ell \lambda[\ell] \rho_A(r) \left\{ i_\ell(\lambda r) k_\ell(\lambda r) + \frac{\lambda r}{[\ell]} [i_\ell(\lambda r) k_{\ell-1}(\lambda r) + i_{\ell+1}(\lambda r) k_\ell(\lambda r)] \right\}, \tag{B10}$$

which with the use of the recurrence relation for i_ℓ in Eq. (B3) can be recast in the form

$$\left[d_{r,r} - \frac{\ell(\ell+1)}{r^2} - \lambda^2\right] y_\ell(r_1;\lambda) = -C_\ell \lambda^2 r \rho_A(r) [k_\ell(\lambda r) i_{\ell-1}(\lambda r) + k_{\ell-1}(\lambda r) i_\ell(\lambda r)]. \tag{B11}$$

This expression for the Poisson equation still looks quite inconvenient because the inhomogeneous term on the right-hand side depends explicitly on the modified spherical Bessel functions for specific values of ℓ. Fortunately, *we have found empirically* the following mathematical identity:

$$z^2 [k_\ell(z) i_{\ell-1}(z) + k_{\ell-1}(z) i_\ell(z)] = \frac{\pi}{2} \quad \forall \ell, \quad z \in \mathbb{Z}, \tag{B12}$$

which, to our knowledge, is not reported in the literature on Bessel functions and it can be transformed to the Bessel pairs $\{J_\alpha, H_\alpha^{(1)}\}$, $\{I_\alpha, K_\alpha\}$, $\{j_\ell, n_\ell\}$ using Eqs. (A2), (A3), and (A4). Now, by introducing this identity in Eq. (B11), the radial screened Poisson equation results in the compact form of Eq. (28).

[1] A. F. Ordóñez-Lasso, J. C. Cardona, and J. L. Sanz-Vicario, Phys. Rev. A **88**, 012702 (2013).
[2] S. Ichimaru, *Plasma Physics: An Introduction to Statistical Physics of Charged Particles* (Benjamin Cummings, Menlo Park, CA, 1986).
[3] P. Debye and E. Hückel, Physik. Z. **24**, 185 (1923).
[4] D. Salzmann, *Atomic Physics in Hot Plasmas* (Oxford University Press, Oxford, UK, 1998).
[5] A. F. Ordóñez-Lasso, F. Martín, and J. L. Sanz-Vicario, Phys. Rev. A **95**, 012504 (2017).
[6] J. M. Ugalde and C. Sarasola, Int. J. Quantum Chem. **62**, 273 (1997).
[7] J. M. Ugalde, C. Sarasola, and X. López, Phys. Rev. A **56**, 1642 (1997).
[8] C. Froese Fischer, T. Brage, and Per Jönsson, *Computational Atomic Structure: An MCHF Approach* (Institute of Physics Publishing, Bristol, PA 1997).
[9] C. W. McCurdy and F. Martín, J. Phys. B **37**, 917 (2004).
[10] I. Sánchez and F. Martín, J. Phys. B **30**, 679 (1997).
[11] Y. V. Vanne and A. Saenz, J. Phys. B **37**, 4101 (2004).
[12] Y. V. Vanne, A. Saenz, A. Dalgarno, R. C. Forrey, P. Froelich, and S. Jonsell, Phys. Rev. A **73**, 062706 (2006).
[13] H. Bachau, E. Cormier, P. Decleva, J. E. Hansen, and F. Martín, Rep. Prog. Phys. **64**, 1815 (2001).
[14] M. Abramowitz and I. A. Stegun, *Handbook of Mathematical Functions with Formulas, Graphs, and Mathematical Tables* (Dover Publications, New York, 1965).
[15] M. Galassi *et al.*, *GNU Scientific Library Reference Manual*, 3rd ed. (2009), https://www.gnu.org/software/gsl/.
[16] I. Sánchez and F. Martín, J. Chem. Phys. **106**, 7720 (1997).
[17] M. Cortés and F. Martín, J. Phys. B **27**, 5741 (1994).
[18] J. C. Cardona, J. L. Sanz-Vicario, and F. Martín, Phys. Rev. A **82**, 022501 (2010).
[19] F. Martín, Phys. Rev. A **48**, 331 (1993).

[20] C. F. Fischer, W. Guo, and Z. Shen, Int. J. Quantum Chem. **42**, 849 (1992).
[21] B. H. Bransden and C. J. Joachain, *Physics of Atoms and Molecules* (Longman Scientific & Technical, New York, 1980).
[22] M. Bylicki, A. Stachów, J. Karwowski, and P. K. Mukherjee, Chem. Phys. **331**, 346 (2007).
[23] F. Morales, C. W. McCurdy, and F. Martín, Phys. Rev. A **73**, 014702 (2006).
[24] C. Joachain, *Quantum Collision Theory* (North-Holland, New York, 1975).
[25] G. B. Arfken, H. Weber, and F. E. Harris, *Mathematical Methods for Physicists* (Academic Press, New York, 2012).